

Snow and glacier investigations using hyperspectral data in the Himalaya

H. S. Negi^{1,*}, Chander Shekhar¹ and S. K. Singh²

¹Snow and Avalanche Study Establishment, Him Parisar, Sector-37A, Chandigarh 160 036, India

²Space Applications Centre, ISRO, Ahmedabad 380 015, India

This article presents highlights of the research work done in hyperspectral remote sensing in the Himalayan cryosphere. Hyperspectral radiometric investigations conducted at different field locations of NW Himalaya and cold laboratory are discussed. Spectral signatures were collected for varying snow grain size, contamination, liquid water content, vegetation/soil-mixed snow, glacier ice, moraines and other ambient objects. The important wavelengths for snow applications are found to be 440, 550, 590, 660, 860, 1050, 1240 and 1650 nm. Further, the retrieval of snow parameters such as grain size, spectral albedo and snow contamination using imaging data at the above wavelength channels is discussed. Wavelengths 550, 1240 and 1660 nm are found to be useful for discriminating different glacier features. Limitations in hyperspectral remote sensing such as availability of imaging data, rugged topography and further research issues such as multi-sensor mapping and data fusion, multi-angle measurements, 3D adjacency effect and improved algorithms for quantitative retrieval of contaminants are identified.

Keywords: Albedo, hyperspectral, hyperion, reflectance, snow cover monitoring, spectroradiometer.

Introduction

SNOW and glaciers are important natural resources in the Himalaya. These are the potential sources of major rivers and have an influence on melt run-off, regional climate, winter tourism, strategic planning and other developmental activities. In addition, many hazards are also associated with snow cover and glaciers such as avalanches, glacial lake outburst flood (GLOF), crevasses and permafrost hazards. Therefore, monitoring of Himalayan cryosphere is important for the above applications. The Himalaya has rugged terrain and harsh climatic conditions and hence conventional field-based methods are difficult to use. Remote sensing has emerged as an alternative method for mapping and monitoring of vast, rugged and remote snow-covered areas¹.

Many studies have been performed globally on the mapping of snow cover using different methods and optical sensors²⁻¹⁰. In addition, many studies have been conducted on snow cover mapping in the Himalaya using optical satellite sensors¹¹⁻¹⁷. Delineation of glacier extent is manually generated by digitization due to non-availability of multispectral data or when glaciers are covered by thick debris¹⁸⁻²¹. Automated glacier mapping was conducted for a large number of glaciers using ratio techniques from multispectral data^{22,23}. Unsupervised²⁴, supervised classification²⁵, fuzzy set theory²⁶ and spectral unmixing²⁷ have also been used for the mapping of glaciers.

In addition to mapping, monitoring of snow characteristics is important for many applications. A few snow cover characteristics such as snow grain size, albedo, specific surface area (SSA) and snow contamination by soot/dust are retrieved using inversion techniques from multispectral satellite data²⁸⁻³⁹. Nolin⁴⁰ highlighted the advancements in remote sensing sensors and analysis techniques of seasonal snow. Different glacier parameters such as glacier area, length, albedo, equilibrium line altitude (ELA), accumulation/ablation rates, accumulation area ratio (AAR) and mass balance gradient have been discussed by Racoviteanu *et al.*⁴¹ using optical remote sensing data. Quincey *et al.*⁴² demonstrated integration of different remote sensing datasets for ice-sheet information such as ice-sheet dynamics and volume changes, melt patterns and formation and drainage of supra- and subglacial lakes.

The hyperspectral sensors capture data in contiguous narrow bands of the electromagnetic spectrum and allow whole spectral curves to be recorded with individual absorption features. Therefore, hyperspectral remote sensing provides information related to surface material that can be exploited to characterize, quantify and perform automated detection of the targets of interest. In this article, we briefly review applications of hyperspectral spectroscopy and imaging data for the Himalayan cryosphere.

Hyperspectral remote sensing for snow and glaciers

The spectral region between 350 and 2500 nm is called the reflective part of the spectrum. The reflectance of

*For correspondence. (e-mail: hs.negi@sase.drdo.in)

snow cover results from contributions of different parameters, namely snow grain size, moisture, contamination, snow depth, sensor and solar zenith angle and cloud cover^{43–48}. Numerous studies have been performed by different researchers on the spectral properties of snow in the optical region^{49–53}.

Nolin and Dozier⁵⁴ described the quantitative estimates of snow grain size from snow reflectance at 1030 nm from Airborne Visible/Infrared Imaging Spectrometer (AVIRIS) data using the DISORT model⁵⁵. Painter *et al.*⁵⁶ retrieved snow grain size at sub-pixel resolution from AVIRIS data using a linear spectral unmixing method. Nolin and Dozier⁵⁷ described snow grain size using continuum across the entire 1030 nm absorption feature from AVIRIS data. Li *et al.*⁵⁸ retrieved snow grain size from multiple wavelengths of 860, 1050, 1240 and 1730 nm from AVIRIS data and found that it depends on wavelength of observation. Painter *et al.*⁵⁹ estimated sub-pixel snow cover and snow grain size using multiple end-member spectral mixtures with a spectral library of snow, vegetation, rock and soil. They derived snow spectral end-members of varying grain size from a radiative transfer model. Green *et al.*⁶⁰ showed the abundance of the three phases of water in an environment that includes melting snow, basing the analysis on the spectral shift in the absorption coefficient between water vapour, liquid water and ice at 940, 980 and 1030 nm respectively, from AVIRIS data. Painter and Dozier⁶¹ showed the effect of anisotropic directional reflectance on the mapping of snow properties from imaging spectrometer data. Molotch and Bales⁶² used snow surface albedo from AVIRIS, and its influence on snowmelt timing and magnitude using a net radiation/temperature index snowmelt model for a series of satellite-based snow covered area scenes and on-site snow surveys. Dozier *et al.*⁶³ reviewed the interpretation of snow properties from imaging spectrometry such as fractional snow-covered area and snow albedo, which are affected by grain size and absorbing impurities (dust and red algae) and snow wetness in the near-surface layer. They also described the application of methods developed with imaging data to multispectral sensors, specifically MODIS. Painter *et al.*⁶⁴ described and validated an algorithm suite (Imaging Spectrometer-Snow Albedo and Radiative Forcing (IS-SnARF)) that provides quantitative retrievals of snow grain size, snow albedo and radiative forcing by light-absorbing impurities in snow and ice from AVIRIS data in the Senator Beck Basin, Colorado, USA. Recently, NASA has launched a mission of Airborne Snow Observatory (ASO), which consists of an imaging spectrometer and a scanning lidar system used to quantify snow water equivalent and snow albedo. This mission, known as the ASO demonstration mission 1, flies over river basins of California and the Rocky Mountains and will be useful in better control and planning for water management⁶⁵.

Casey *et al.*⁶⁶ have discussed composition of supraglacial debris using hyperspectral data that further helps improve, supplement and potentially reduce errors associated with glacier debris radiative property, composition, areal extent and mass flux quantifications. So far hyperspectral data have not been explored much for glacier applications.

Hyperspectral spectroscopy in the Himalaya

Major rivers of North India originate from the Himalaya. It is important to know the periods and magnitude of snow melt for hydrological applications. Better estimation of snow grain size, albedo and snow cover area is needed to study regional climatic variations. Recent studies have shown the effects of black carbon over the Himalayan cryosphere⁶⁷. Therefore, it is essential to understand the effect of contaminants such as black carbon, dust, etc. on snow albedo. Also, knowledge of snow surface conditions is an important input in avalanche prediction. To retrieve all the above required information from remote sensing sensors, it is essential to understand the hyperspectral spectroscopy of different target objects. The field-based spectral measurements are useful in calibration of remote sensing sensors, development/testing of models relating to remote sensing data and predicting the optimum spectral bands for particular applications^{68,69}.

Instrument and experiment plan

Reflectance measurements were carried out for different kinds of snow and ice using a hyperspectral spectroradiometer. Experiments were conducted at different field locations of the western Himalaya as well as in a controlled environment at the cold laboratory of Snow and Avalanche Study Establishment (SASE), Manali (Figure 1). Analytical Spectral Devices Inc. (ASD) spectroradiometer in the spectral wavelength range 350–2500 nm with 3 nm spectral resolution in VIS and 10 nm spectral resolution in SWIR region was used⁷⁰. All the reflectance observations were carried out at nadir (i.e. viewing zenith angle at 0°).

Figure 2a shows the field set-up of the spectroradiometer with collateral instruments such as crystal gauge, moisturemeter, albedometer, density meter and thermometers. Snow grain sizes were measured as average maximum lengths (equivalent grain diameter (EGD)) using a crystal gauge with a magnifying hand lens in field. These were found in different categories as fine (<0.5 mm), medium (0.5–1.0 mm) and coarse (1.0–2.0 mm). To measure the liquid water content in snow cover, a dielectric moisture meter with a flat capacitive sensor⁷¹ or snow fork⁷² was used. For contamination experiments, contaminants such as black charcoal, soil and wood ash were used. The samples were prepared into different categories of weight

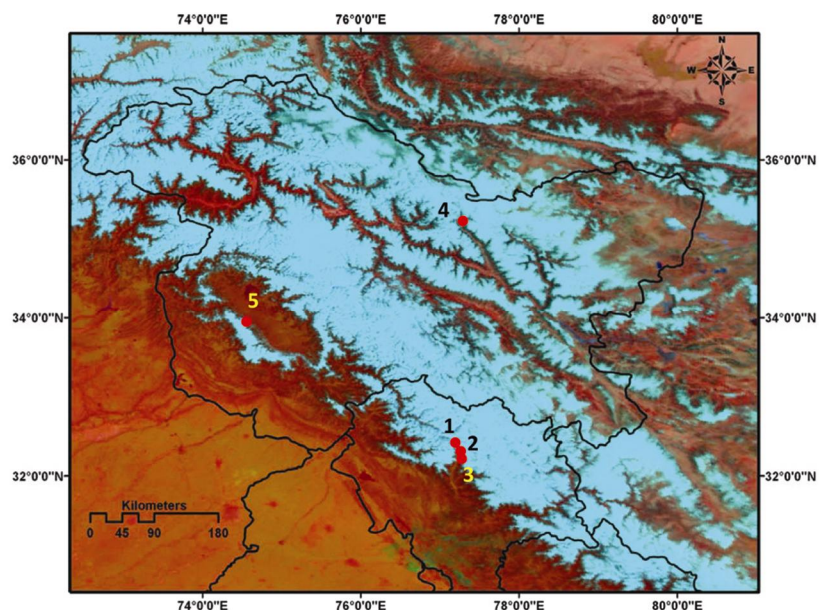


Figure 1. Map of western Himalaya showing locations of field investigation using spectroradiometer: 1, Dhundi; 2, Solang; 3, Manali; 4, Siachen Glacier; 5, Gulmarg.

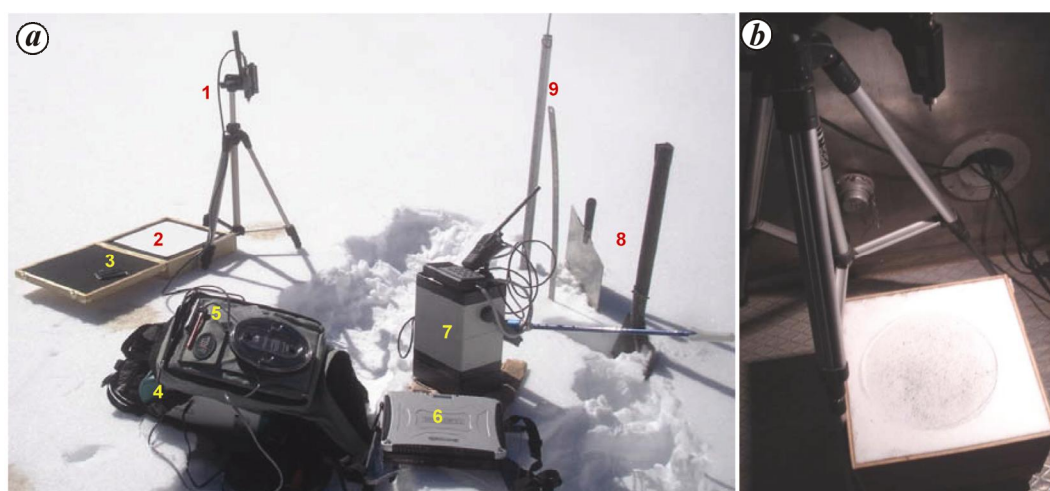


Figure 2. *a*, Field set-up of spectroradiometer (1, Fore optic cable with stand; 2, Reference panel; 3, GPS; 4, Spectroradiometer main unit; 5, Crystal gauge, micro mike, snow thermometer; 6, Display unit; 7, Snow fork; 8, Snow shovel and cutting plate and 9, Snow depth rod and measuring scale). *b*, Cold laboratory set-up for contamination study.

and spread on the snow surface. The instrument fore optics sensor was kept at a height so that it can view the contaminated snow cover area. To understand the effect of the concentration (mg/g) of contaminants on snow reflectance, the experiments were conducted in the cold laboratory, SASE, Manali. The cold chamber was maintained at -10°C to avoid bond formations in snow crystals. A calibrated lamp was used as the light source for illumination. A wooden box of dimensions $30 \times 30 \times 20 \text{ cm}^3$ was used for snow sample of known grain size ($<1 \text{ mm}$) and density (0.3 g/cc). A hollow cylinder of radius 10 cm and depth 20 cm was used for volumetric

mixing and restricting the contamination to a fixed field of view of the radiometer, which was removed after a known amount of contamination mixing. The cold laboratory set-up for contamination study is shown in Figure 2 *b*. To understand the impact of linear mixing of different objects on reflectance, different proportions of snow-vegetation, snow-soil and soil-vegetation were made in a fixed field-of-view of 25° . Different proportions of snow were covered by vegetation/soil (i.e. 25%, 50%, 75% and 100% successively) and reflectance was observed. Spectral signatures of glacier snow, ice, moraines, etc. were collected in the Siachen Glacier.

Table 1. Hyperspectral spectroscopy studies conducted in the Himalayan cryosphere

Experiment	Objective(s)	Reference
Different types of contamination and mixed objects	Effect of contamination and mixed pixel in snow cover mapping	75
Snow grain size, contamination, moisture, snow depth, slope/aspect	Identification of suitable wavelengths for snow characterization and snow indices	74
Snow grain size and contamination	Hyperspectral analysis to understand the grain size and contamination	79
Reflectance measurements of new and old snow	Quantitative retrieval of snow albedo and effective grain size	73
Coal and soil contamination	Hyperspectral analysis of coal and soil contamination	80
Contamination in volume mixing	Effect of contaminants concentration on snow reflectance	Present study
Spectral signatures of glacier ice and moraines	Identification of glacier characteristics	Present study

Spectral reflectance measurements

The work done by different researchers in the area of spectral reflectance measurements in the Himalayan cryosphere is summarized in Table 1. Details of experiments conducted at different field locations and snow and meteorological parameters measured at the time of field experiments are given in Table 2.

The spectral reflectance decreases with increase in grain size which represents the range for the fine new snow to coarse spring snow in the NIR region (Figure 3a). The maximum variations in reflectance or sensitive wavelengths were observed as 1050 and 1240 nm in the NIR region, as these wavelengths are more absorptive due to the presence of ice. The grain size retrievals using these wavelengths have been discussed by Negi and Kokhanovsky⁷³ for Himalayan snow. Presently, there is a gap in parametrization between physical grain size (i.e. EGD measured using crystal gauge with micro mike) and optical grain data measured from optical sensors. This is required for the validation and retrieval of spectral albedo from grain size. Alternatively, we suggest that snow grain size measurements should be collected using light reflectance instrument or SSA measurements on the snow surface. As the liquid water appear in snow, the maximum variations in spectral reflectance were observed around wavelengths 980 and 1160 nm (ref. 74). This shows that as the H₂O phase changes from solid to liquid both the absorption peaks shift to shorter wavelengths. Detection of such shift in absorption peak with increase in moisture is possible only with the hyperspectral data. However, quantification of the volume of liquid in snow (%) from a single spectral plot needs more experiments.

The effect of different types of contamination on spectral reflectance of snow is shown in Figure 3b (ref. 75). It can be observed that contaminants considerably decrease the snow spectral reflectance in the visible and NIR region. The same amount of contaminant (1 mg/cm² on the snow surface) decreases the snow albedo by approximately 30%, 55% and 66% for soil, ash and coal contamination respectively, at wavelength 412 nm. The average decrease in reflectance is approximately 25%, 50% and

65% in visible region for 1 mg/cm² soil, ash and coal contaminants respectively. Figure 3c and d shows the drop in hemispherical directional reflectance factor of snow with increase in the level of contamination concentration (mg/g) due to coal (black carbon) and soil respectively. The drop in reflectance for the same concentration is observed to be significant in the case of coal contamination compared to soil contamination at all wavelengths in the visible region. Details of hyperspectral analysis of contamination are discussed later in the text.

To address the issue of snow mixed with vegetation in mountainous areas, experiments were conducted with different linear mixtures of snow and vegetation. The hyperspectral measurements of snow and vegetation mixing are shown in Figure 3e. The leaves of pine tree were selected for mixing, as coniferous vegetation is generally found in the high altitude snow bound regions. The presence of vegetation in snow can be observed by the peak in green and NIR wavelength regions of the spectral reflectance. To check the suitability of linear mixing model (LMM)⁷⁶ for sub-pixel mapping of snow, the mixed spectra were generated using LMM. These generated spectra are found to be similar to experimental observed spectra, but the magnitudes are different in the visible region. The error analysis shows that as the proportion of vegetation mixing increases, the error also increases in the visible region. This can be attributed to multiple scattering due to vegetation. However, in the NIR region there was no significant variation in the error due to snow – vegetation mixing and beyond that in SWIR region the error was observed due to low signal-to-noise (SNR) ratio. These experiments show that one can retrieve grain size correctly at 1050 nm wavelength even from the snow cover of vegetated area (Figure 3e). Similar experiments were conducted for soil mixing, but more experiments on LMM for snow–soil mixing are needed to reach some conclusions.

Spectral signatures collected near Siachen glacier are presented in Figure 3f. The high reflectance of snow in the visible region can be well distinguished from other target objects on the glacier. Glacier ice (blue, white, black, transparent) also has maximum reflectance in the

Table 2. Spectroradiometer experiments conducted in the western Himalayan region with ancillary information

Location/mountain range	Type of signature	Date/time (LMT)/SZA (°)	T_s	Snow and meteorological information					Remark
				GT	GS	ρ	SD	CC	
Bhang, Manali, Himachal Pradesh (HP) Altitude: 1951 m Pir Panjal Range	Snow grain size	29 January 2005/10 : 30/57.6	-2.0	Stellar	<0.5	0.13	27	0	New snow of day 1
		29 January 2005/10 : 45/54.9	-1.5	Rounded	0.5-1.0	0.18	26	0	
		29 January 2005/11 : 50/51.0	0	Rounded	1.0-2.0	0.32	23	0	
Dhundi, HP Altitude: 2851 m Pir Panjal Range	Soil contamination, ash contamination and coal contamination on snow surface (mg/cm ²)	27 February 2006/11 : 45/42.4	0	Rounded	<1.0	0.14	100	0	27 February 2006 is day 1 after fresh snowfall; vegetation: pine leaves; soil: brown fine-grained
		28 February 2006/09 : 20/61.0	-1.0	MF layer of 3 cm		0.18	100	0	
		28 February 2006/10 : 20/51.5	0	MF layer of 3 cm		0.19	100	0	
SASE, Manali Cold Laboratory	Mixed objects: linear mixing of snow-vegetation and snow-soil	28 February 2006	0	Melting	1.0-2.0	0.23	100	0	Coal and soil contamination concentration in snow (mg/g)
		27 February 2006	0	Rounded	0.5-1.0	0.23	100	0	
		13 March 2010	-10	Rounded	<1.0 mm	0.3	20	-	
Siachen Glacier, J&K Altitude: 4000 m Karakoram Range	Different kinds of snow, ice, moraines, frozen river, barren land, etc.	21 February 2003, 10 : 40 (snow)							Only qualitative information of various glacier features was collected
		Time interval 09 : 00-12 : 00							
Solang, HP Altitude: 2455 m Pir Panjal Range	Spectral albedo measurements of snow	19 February 2008, hourly temporal measurements		Negi and Kokhanovsky ⁷³					Old/metamorphosed snow

SZA, Solar zenith angle; T_s , Snow surface temperature (°C); GT, Grain type (MF, Melt freeze); GS, Grain size (mm); ρ , Top layer density (g/cm³); SD, Snow thickness (cm); CC, Cloud cover (octa).

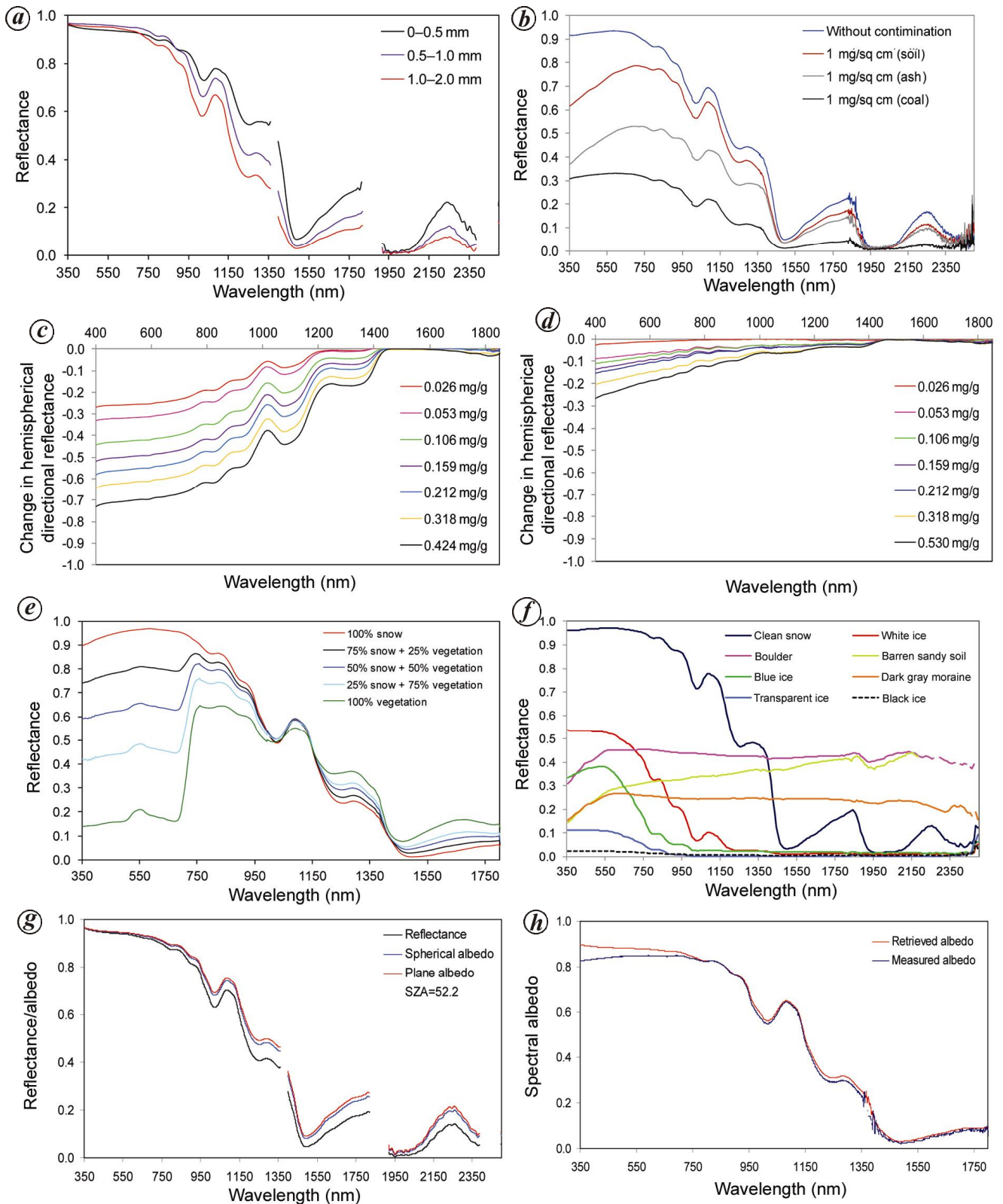


Figure 3. *a*, Spectral reflectance of different types of snow grains. *b*, Spectral reflectance of different type of contaminants on snow surface. *c*, Drop in spectral reflectance of snow due to different level of coal concentration. *d*, Drop in spectral reflectance of snow due to different level of soil concentration. *e*, Spectral reflectance of different proportions of vegetation mixing⁷⁵. *f*, Spectral reflectance of different glacier features. *g*, Measured spectral reflectance versus simulated spectral albedo of snow⁷³. *h*, Simulated spectral albedo versus measured spectral albedo of snow⁷³.

visible region, which becomes almost zero beyond 1500 nm due to high absorption of ice in the SWIR region. Black ice signatures are found to be close to water as it absorbs completely beyond the NIR region. The difference in spectral reflectance of ice and snow in VNIR and SWIR wavelengths is useful to make automated mapping of debris-free glaciers using NDSI or NDSII⁷⁷, where

$$\text{NDSI} = \frac{\text{Reflectance (green)} - \text{Reflectance (SWIR)}}{\text{Reflectance (green)} + \text{Reflectance (SWIR)}}$$

and

$$\text{NDSII} = \frac{\text{Reflectance (red)} - \text{Reflectance (SWIR)}}{\text{Reflectance (red)} + \text{Reflectance (SWIR)}}$$

Due to debris deposition on the glacier surface, spectral reflectance starts increasing in the visible and remains high in NIR and SWIR regions compared to snow and ice signatures. The mineral composition of debris can be identified with the help of hyperspectral sensors wavelengths as discussed in detail by Casey *et al.*⁶⁶. This indirect method involving identification of mineral composition of debris using hyperspectral data helps in the mapping of debris-covered glaciers. Thus extracting debris cover information based on mineral composition and utilizing specific mineral absorption characteristics by the use of hyperspectral sensors opens up new avenues to study debris covered glaciers using hyperspectral data.

The reflectance measurements made are reflectance factors which consider target object as a lambertian surface. Therefore, to consider the effect of object anisotropy, there is a need to determine spectral albedo or measure it directly. For the retrieval of snow spectral albedo, Negi and Kokhanovsky⁷³ made use of spectral reflectance measurements of Himalayan snow (Figure 3g). The asymptotic radiative transfer (ART) theory⁷⁸ was applied to retrieve the spectral albedos (plane and spherical). In addition, spectral albedo measurements were directly collected for different kinds of snow and compared with the above simulated spectral albedo. A good agreement was observed with $\pm 10\%$ difference between the retrieved plane albedo and the measured spectral albedo of snow (Figure 3h)⁷³.

Hyperspectral analysis of spectral reflectance

Figure 4a shows the change in reflectance (%) at 440 nm due to coal and soil concentration in snow. It is observed that reflectance drops to approximately 50% by addition of 0.16 mg/g coal contaminant. However, for the same concentration of soil contamination the reflectance drops by approximately 12%. However, this reduction in reflectance

is not linear and further analysis is needed to quantify concentration. Since the visible wavelengths are more sensitive to atmospheric effect, quantification of concentration with remote sensing using the visible channel is not straightforward. The following hyperspectral analysis methodology may help in this regard.

Singh *et al.*⁷⁹ have analysed snow reflectance data to understand the effect of soil contamination and grain size. They have defined and analysed shape, size and strength of absorption peak at 1025 nm after continuum removal and observed that depth of the peak at 1025 nm increases with increase in grain size and decreases with increase in the amount of soil contamination (snow grain size 0.1–0.6 mm during contamination experiment). Shift in the peak of first derivative of reflectance and changes like right asymmetry to left asymmetry in curve shape with increase in contamination have also been observed. It was suggested by these authors that this type of analysis based on parameters of spectral curve has the potential to identify the influence of contamination and grain size-based metamorphism using hyperspectral imaging. It has also been mentioned that soil contaminants reduce albedo only up to a certain amount of the contaminant, after which there is saturation, i.e. no further reduction with addition of soil contaminant.

Similar spectral curve parameters for hyperspectral analysis along with percentage change in reflectance at selected wavelengths (575, 585, 695, 745, 1085, 1645, 2265 nm) have also been analysed for soil and coal contamination in snow by Singh *et al.*⁸⁰. Relative strength of peak followed an increasing trend with increase in either soil or coal contaminants and the increase was significant for low coal contamination. Change from right to left asymmetry in the peak curve at 1025 nm was significant only for coal contaminants. Width of peak was not significant for both types of contamination. Noticeable shift in peak was observed for soil contamination compared to coal contamination. Coal contaminants resulted in greater reduction in snow albedo than soil. The authors suggested that a combination of these parameters may provide a way to discriminate the soil- or coal-contaminated snow.

This analysis needs to be implemented on the hyperspectral image to check the suggestions of the authors as a number of intervening parameters like atmospheric corrections, topographic corrections, etc. pose a problem for this kind of analysis in the rugged and cloud-covered Himalaya. The quest still remains to distinguish between soil and coal-contaminated spectra and quantify them using such an analysis, which needs further correction for erroneous interpretations as pointed out by Painter⁸¹. There appears to be a scope of improvement for better understanding the effect of contamination and other intriguing parameters on snow reflectance signatures.

To distinguish various glacier features like moraines/boulders, snow and ice, some of the ratio and index techniques were attempted by various researchers. These are

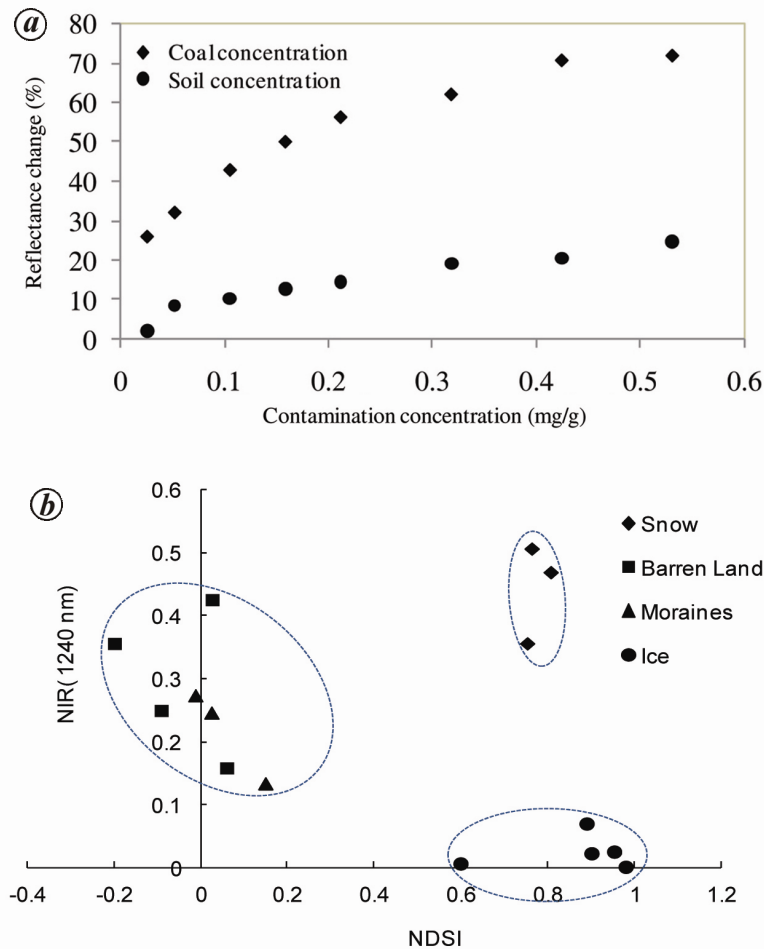


Figure 4. *a*, Change in reflectance due to contamination concentration (mg/g) with respect to clean snow at 440 nm wavelength. *b*, Analysis of glacier feature signatures (NDSI versus reflectance at 1240 nm).

SWIR/red, SWIR/NIR, NIR/red, NDSI and NDSII. To select the most suitable wavelengths for discriminating various glacial features (snow, ice, moraine and barren land), a selectivity analysis, i.e. variation of reflectance at NIR wavelengths with NDSI was attempted. In a scatter plot the spectral distances were calculated among features of interest. We considered average values of various signatures at individual wavelengths for analysis and spectral distances were calculated based on these average values. We found that at a specific wavelength of 1240 nm, the spectral distances with NDSI were large as compared to other wavelengths and thus the reflectance at three wavelengths 550, 1660 nm (for NDSI), and 1240 nm can be used to discriminate different glacier features (Figure 4 *b*). Further, this observation is required to be validated on satellite data.

Hyperspectral imaging in the Himalaya

Availability of imaging data over the Himalayan region is a major limitation. The only data available were from spaceborne EO-1, Hyperion sensor. Spectral albedo,

snow grain size, patchy and contaminated snow cover were retrieved from Hyperion data. The reflectance generally retrieved from the satellite collected radiances is bidirectional reflectance, where normally the target is considered as a Lambertian. Therefore, to consider the effect of object anisotropy, there is a need to determine spectral albedo. Further, spectral albedo is required for retrieving different snow cover parameters and broadband albedo. In the Himalaya, Negi and Kokhanovsky⁸² retrieved spectral albedo from satellite reflectance using asymptotic radiative transfer (ART) theory⁷⁸. The main advantage of ART theory is its simple approach of using analytical equations compared to other radiative transfer theories for retrieving the snow characteristics. This theory is valid only for weakly absorbing media like snow, cloud, etc. and can generate the spectral albedo from a single reflectance measurement. To our knowledge no spectral albedo product is presently available on a daily basis for the Himalayan region, where the albedo is highly variable due to temperature conditions varying with altitude and slope and snow metamorphism proceeds fast. But the advantage of the ART technique makes it suitable to retrieve spectral albedo on a daily basis for the Himalayan

region. The methodology of retrieving snow spectral albedo has been discussed by Negi and Kokhanovsky^{73,82}.

Snow grain size is an important parameter which indicates the advancement in the snow metamorphism and can be used to retrieve albedo. In combination with snow surface temperature, it provides information about melting snow. In snow avalanches it can be related to the stability of snowpack, as fine-grain snow cover has more strength than coarse-grain snow. To make the methodology operational, Negi and Kokhanovsky⁸² used only five spectral bands (440, 500, 1050, 1240 and 1650 nm) of the Hyperion data for retrieval of snow parameters to reduce the time and memory space in processing. The bi-spectral method, i.e. one in visible and another in NIR region (440 and 1050/1240 nm) proposed by Kokhanovsky *et al.*³⁴ was used to retrieve snow grain size. The use of visible channel takes care of absorption due to soot (if any) in NIR channel. Negi and Kokhanovsky⁸² observed that grain size using NIR wavelength 1240 nm can work well for clean and dry snow of the Himalaya.

Negi *et al.*⁸³ compared the snow grain size estimated using the spectral angle mapper (SAM), grain index⁷⁴ and ART theory methods for a part of the Himalayan region from Hyperion data. The SAM and grain index methods were established as alternatives to obtain the snow grain size for applications where quantitative grain sizes are not required. They also identified the vegetation-mixed and contamination/patchy (soil-mixed) snow cover areas in Hyperion scenes and the results were supported using high resolution images for snow conditions of the region. The recent work of Kokhanovsky⁸⁴ relating spectral albedo to retrieve the soot and dust concentrations in snow may be useful for the Himalayan cryosphere.

Conclusion and future prospects

Continuous field-based spectral measurements have been conducted in the Himalayan cryosphere which are useful to develop new algorithms for retrieving various snow and glacier parameters. Apart from estimation of snow grain size, contamination, fractional snow cover area, hyperspectral imaging is helpful in accurate estimation of albedo, improved snow cover mapping, timing and magnitude of snow melt to better estimate future water resources, climate forcing, accurate mapping of clean/debris-covered glaciers, glacial hazards, etc. Multi-angle measurements of snow cover may help in identification of different snow surface characteristics such as crusted surface (Sun crust), windblown surface, ripples, sastrugis (derived wind velocities), firn speigel (mirror of ice), surface water rills, avalanche snow, crevasses, etc. In defence applications, it is helpful in camouflage study to devise shelters in security-sensitive areas. Further applications of hyperspectral data are in fusion with lidar data for mapping the terrain variation such as snow water

equivalent, avalanche debris measurement, and debris volume estimation for structural control planning. In addition, fusion of microwave data may help in better estimation and target identification.

Along with the spectral signatures in the reflective part of the spectrum, there is a need of signatures in emissive regions. A systematic study using thermal sensor can help in the estimation of emissivity, snow surface temperature, buried object detection under snow cover, glacier study (debris-covered ice), etc. In hyperspectral remote sensing, availability of imaging data over the Himalayan region is a major limitation. Secondly, rugged terrain is a major challenge for retrieving snow cover information due to 3D adjacency effect, etc. Therefore, there is a need to develop robust and standardized methodologies for pre-processing (atmospheric and topographic corrections) of hyperspectral imaging data for rugged mountainous terrain. Development of radiative transfer-based models for quantitative retrieval of snow characteristics and algorithms for snow and glacier feature identification and classification are needed. SASE has initiated a project on instrumented airborne hyperspectral imaging with lidar and photogrammetry sensors for monitoring of the Himalayan cryosphere. Such a platform may overcome, up to some extent, the research gaps/challenges of imaging data over the Himalayan cryosphere.

1. Konig, M., Winther, J. G. and Isaksson, E., Measuring snow and glacier properties from satellite. *Rev. Geophys.*, 2001, **39**, 1–27.
2. Dozier, J., Schneider, S. R. and McGinnis, J. D. F., Effect of grain size and snow pack water equivalence on visible and near infrared satellite observations of snow. *Water Resour. Res.*, 1981, **17**, 1213–1221.
3. Dozier, J., Snow reflectance from LANDSAT-4 Thematic Mapper. *IEEE Trans. Geosci. Remote Sensing*, 1984, **22**, 323–328.
4. Dozier, J., Spectral signature of alpine snow cover from the Landsat Thematic Mapper. *Remote Sensing Environ.*, 1989, **28**, 9–22.
5. Hall, D. K., Riggs, G. A. and Salomonson, V. V., Development of methods for mapping global snow cover using moderate resolution imaging spectroradiometer data. *Remote Sensing Environ.*, 1995, **54**, 127–140.
6. Hall, D. K., Riggs, G. A., Salomonson, V. V., DiGirolamo, N. E. and Bayr, K. J., MODIS snow cover products. *Remote Sensing Environ.*, 2002, **83**, 181–194.
7. Klein, A. G., Hall, D. K. and Riggs, G. A., Improving snow cover mapping in forests through the use of a canopy reflectance model. *Hydrol. Process.*, 1998, **12**, 1723–1744.
8. Vikhamar, D. and Solberg, R., Snow-cover mapping in forests by constrained linear spectral unmixing of MODIS data. *Remote Sensing Environ.*, 2003, **88**, 309–323.
9. Salomonson, V. V. and Appel, I., Estimating fractional snow-cover from MODIS using the normalised difference snow index. *Remote Sensing Environ.*, 2004, **89**, 351–360.
10. Painter, T. H., Rittger, K., McKenzie, C., Slaughter, P., Davis, R. E. and Dozier, J., Retrieval of sub-pixel snow covered area, grain size, and albedo from MODIS. *Remote Sensing Environ.*, 2009, **113**, 868–879.
11. Gupta, R. P., Haritashya, U. K. and Singh, P., Mapping dry/wet snow cover in the Indian Himalayas using IRS multispectral imagery. *Remote Sensing Environ.*, 2005, **97**, 458–469.

12. Kulkarni, A. V., Singh, S. K., Mathur, P. and Mishra, V. D., Algorithm to monitor snow cover using AWiFS data of RESOURCESAT-1 for the Himalayan region. *Int. J. Remote Sensing*, 2006, **27**, 2449–2457.
13. Kulkarni, A. V., Rathore, B. P., Singh, S. K. and Ajai, Distribution of seasonal snow cover in central and western Himalaya. *Ann. Glaciol.*, 2010, **51**, 123–128.
14. Kulkarni, A. V., Rathore, B. P., Singh, S. K. and Bahuguna, I. M., Understanding changes in the Himalayan cryosphere using remote sensing techniques. *Int. J. Remote Sensing*, 2011, **32**, 601–615.
15. Jain, S. K., Goswami, A. and Saraf, A. K., Accuracy assessment of MODIS, NOAA and IRS data in snow cover mapping under Himalayan conditions. *Int. J. Remote Sensing*, 2008, **29**, 5863–5878.
16. Negi, H. S., Kulkarni, A. V. and Semwal, B. S., Estimation of snow cover distribution in Beas basin, Indian Himalaya using satellite data and ground measurements. *J. Earth Syst. Sci.*, 2009, **118**, 525–538.
17. Immerzeel, W. W., Droogers, P., Jong, S. M. and Bierkens, M. F. P., Large-scale monitoring of snow cover and runoff simulation in Himalayan river basins using remote sensing. *Remote Sensing Environ.*, 2009, **113**, 40–49.
18. Hall, D. K., Bayr, K. J., Schöner, W., Bindenschadler, R. A. and Chien, J. Y. L., Consideration of the errors inherent in mapping historical glacier positions in Austria from the ground and space (1893–2001). *Remote Sensing Environ.*, 2003, **86**(4), 566–577.
19. Paul, F., Changes in glacier area in Tyrol, Austria, between 1969 and 1992 derived from Landsat 5 TM and Austrian glacier inventory data. *Int. J. Remote Sensing*, 2002, **23**(4), 787–799.
20. Paul, F., Huggel, C. and Käab, A., Combining satellite multispectral image data and a digital elevation model for mapping of debris-covered glaciers. *Remote Sensing Environ.*, 2004, **89**(4), 510–518.
21. Kulkarni, A. V., Monitoring Himalayan cryosphere using remote sensing techniques. *J. Indian Inst. Sci.*, 2010, **90**(4), 457–469.
22. Paul, F. and Käab, A., Perspectives on the production of a glacier inventory from multispectral satellite data in the Canadian Arctic: Cumberland Peninsula, Baffin Island. *Ann. Glaciol.*, 2005, **42**, 59–66.
23. Racoviteanu, A. E., Arnaud, Y., Williams, M. W. and Ordoñez, J., Decadal changes in glacier parameters in the Cordillera Blanca, Peru, derived from remote sensing. *J. Glaciol.*, 2008, **54**(186), 499–510.
24. Aniya, M., Sato, H., Naruse, R., Skvarca, P. and Casassa, G., The use of satellite and airborne imagery to inventory outlet glaciers of the Southern Patagonia Ice field, South America. *Photogramm. Eng. Remote Sensing*, 1996, **62**(12), 1361–1369.
25. Li, Z., Wenxin, S. and Qunzhu, Z., Measurements of glacier variation in the Tibetan Plateau using Landsat data. *Remote Sensing Environ.*, 1998, **63**, 258–264.
26. Binaghi, E., Madella, P., Montesano, M. P. and Rampini, A., Fuzzy contextual classification of multisource remote sensing images. *IEEE Trans. Geosci. Remote Sensing*, 1997, **35**(2), 326–339.
27. Klein, A. G. and Isacks, B. L., Spectral mixture analysis of Landsat Thematic Mapper images applied to the detection of the transient snowline on tropical Andean glaciers. *Global Planet. Change*, 1999, **22**, 139–154.
28. Dozier, J., Spectral signature of alpine snow cover from the Landsat Thematic Mapper. *Remote Sensing Environ.*, 1989, **28**, 9–22.
29. Bourdelles, B. and Fily, M., Snow grain-size determination from Landsat imagery over Terre Adelie, Antarctica. *Ann. Glaciol.*, 1993, **17**, 86–92.
30. Fily, M., Bourdelles, B., Dedieu, J. P. and Sergent, C., Comparison of *in situ* and Landsat thematic mapper derived snow grain characteristics in the Alps. *Remote Sensing Environ.*, 1997, **59**, 452–460.
31. Hori, M., Aoki, T., Stamnes, K., Chen, B. and Li, W., Preliminary validation of the GLI cryosphere algorithms with MODIS daytime data. *Polar Meteorol. Glaciol.*, 2001, **15**, 1–20.
32. Painter, T. H., Dozier, J., Roberts, D. A., Davis, R. E. and Greene, R. O., Retrieval of sub-pixel snow-covered area and grain size from imaging spectrometer data. *Remote Sensing Environ.*, 2003, **85**, 64–77.
33. Kokhanovsky, A. A., Aoki, T., Hachikubo, A., Hori, M. and Zege, E. P., Reflective properties of natural snow: approximate asymptotic theory versus *in situ* measurements. *IEEE Trans. Geosci. Remote Sensing*, 2005, **43**, 1529–1535.
34. Kokhanovsky, A. *et al.*, Sizing snow grains using backscattered solar light. *Int. J. Remote Sensing*, 2011, **32**(22), 6975–7008.
35. Tedesco, M. and Kokhanovsky, A. A., The semi-analytical snow retrieval algorithm and its application to MODIS data. *Remote Sensing Environ.*, 2007, **110**, 317–331.
36. Lyapustin, A., Tedesco, M., Wang, Y., Aoki, T., Hori, M. and Kokhanovsky, A., Retrieval of snow grain size over Greenland from MODIS. *Remote Sensing Environ.*, 2009, **113**, 1976–1987.
37. Kokhanovsky, A. and Schreier, M., The determination of snow specific surface area, albedo and effective grain size using AATSR space-borne measurements. *Int. J. Remote Sensing*, 2009, **30**, 919–933.
38. Zege, E. P., Katsev, I. L., Malinka, A. V., Prikhach, A. S., Heygster, G. and Wiebe, H., Algorithm for retrieval of the effective snow grain size and pollution amount from satellite measurements. *Remote Sensing Environ.*, 2011, **115**, 2674–2685.
39. Mary, A. *et al.*, Intercomparison of retrieval algorithms for the specific surface area of snow from near-infrared satellite data in mountainous terrain, and comparison with the output of a semi-distributed snowpack model. *Cryosphere*, 2013, **7**, 741–761.
40. Nolin, A. W., Recent advances in remote sensing of seasonal snow. *J. Glaciol.*, 2010, **56**(200), 1141–1149.
41. Racoviteanu, A. E., Williams, M. W. and Barry, R. G., Optical remote sensing of glacier characteristics: a review with focus on the Himalaya. *Sensors*, 2008, **8**, 3355–3383.
42. Quincey, D., Luckman, A. and Benn, D., Quantification of Everest region glacier velocities between 1992 and 2002, using satellite radar inter-ferometry and feature tracking. *J. Glaciol.*, 2009, **55**, 596–606.
43. Wiscombe, W. J. and Warren, S. G., A model for the spectral albedo of snow-I: pure snow. *J. Atmos. Sci.*, 1980, **37**, 2712–2733.
44. Warren, S. G., Optical properties of snow. *Rev. Geophys. Space Phys.*, 1982, **20**(1), 67–89.
45. Dozier, J., Spectral signature of alpine snow cover from the Landsat Thematic Mapper. *Remote Sensing Environ.*, 1989, **28**, 9–22.
46. Winther, J. G. *et al.*, Snow research in Svalbard – an overview. *Polar Res.*, 2003, **22**, 125–144.
47. Casacchia, R., Lauta, F., Salvatori, R., Cagnati, A., Valt, M. and Ørbæk, J. B., Radiometric investigation of different snow covers in Svalbard. *Polar Res.*, 2001, **20**(1), 13–22.
48. Takeuchi, N., Temporal and spatial variations in spectral reflectance and characteristics of surface dust on Gulkana Glacier, Alaska Range. *J. Glaciol.*, 2009, **55**(192), 701–709.
49. Bohren, C. F. and Barkstrom, B. R., Theory of the optical properties of snow. *J. Geophys. Res.*, 1974, **79**(30), 4527–4535.
50. Warren, S. G. and Wiscombe, W. J., A model for the spectral albedo of snow-II: snow containing atmospheric aerosols. *J. Atmos. Sci.*, 1980, **37**, 2734–2745.
51. Greenfell, T. C., Perovich, D. K. and Ogren, J. A., Spectral albedos of an Alpine Snowpack. *Cold Regions Sci. Technol.*, 1981, **4**, 121–127.
52. Warren, S. G., Optical properties of snow. *Rev. Geophys. Space Phys.*, 1982, **20**, 67–89.
53. Aoki, T., Fukabori, M., Hachikubo, A., Tachibana, Y. and Nishio, F., Effects of snow physical parameters on spectral albedo and bi-directional reflectance of snow surface. *J. Geophys. Res.*, 2000, **105**(D8), 10219–10236.
54. Nolin, A. W. and Dozier, J., Estimating snow grain size using AVIRIS data. *Remote Sensing Environ.*, 1993, **44**, 231–238.

55. Stamnes, K., Tsay, S. C., Wiscombe, W. and Jayaweera, K., Numerically stable algorithm for discrete-ordinate-method radiative transfer in multiple scattering and emitting layered media. *Appl. Optics*, 1988, **27**, 2502–2509.
56. Painter, T. H., Roberts, D. A., Green, R. O. and Dozier, J., The effect of grain size on spectral mixture analysis of snow-covered area from AVIRIS data. *Remote Sensing Environ.*, 1998, **65**, 320–332.
57. Nolin, A. W. and Dozier, J., A hyperspectral method for remotely sensing the grain size of snow. *Remote Sensing Environ.*, 2000, **74**, 207–216.
58. Li, W., Stamnes, K., Chen, B. and Xiong, X., Snow grain size retrieved from near-infrared radiances at multiple wavelengths. *Geophys. Res. Lett.*, 2001, **28**, 1699–1702.
59. Painter, T. H., Dozier, J., Roberts, D. A., Davis, R. E. and Greene, R. O., Retrieval of sub-pixel snow-covered area and grain size from imaging spectrometer data. *Remote Sensing Environ.*, 2003, **85**, 64–77.
60. Green, R. O., Painter, T. H., Roberts, D. A. and Dozier, J., Measuring the expressed abundance of the three phases of water with an imaging spectrometer over melting snow. *Water Resour. Res.*, 2006, **42**, W10402.
61. Painter, T. H. and Dozier, J., The effect of anisotropic reflectance on imaging spectroscopy of snow properties. *Remote Sensing Environ.*, 2004, **89**, 409–422.
62. Molotch, N. P. and Bales, R. C., Comparison of ground-based and airborne snow-surface albedo parameterizations in an alpine watershed: impact on snowpack mass balance. *Water Resour. Res.*, 2006, **42**, doi: 10.1029/2005WR004522.
63. Dozier, J., Green, R. O., Nolin, A. W. and Painter, T. H., Interpretation of snow properties from imaging spectrometry. *Remote Sensing Environ.*, 2009, **113**, 25–37.
64. Painter, T. H., Seidel, F. C., Bryant, A. C., Skiles, S. M. and Rittger, K., Imaging spectroscopy of albedo and radiative forcing by light absorbing impurities in mountain snow. *J. Geophys. Res.: Atmospheres*, 2013, **118**, 9511–9523.
65. <http://www.aso.jpl.nasa.gov>
66. Casey, K. A., Kaab, A. and Benn, D. I., Geochemical characterization of supraglacial debris via *in situ* and optical remote sensing methods: a case study in Khumbu Himalaya, Nepal. *Cryosphere*, 2012, **6**, 85–100.
67. Ming, J., Cachier, H., Xiao, C., Qin, D., Kang, S., Hou, S. and Xu, J., Black carbon record based on a shallow Himalayan ice core and its climatic implications. *Atmos. Chem. Phys.*, 2008, **8**, 1343–1352.
68. Milton, E. J., Principles of field spectroscopy – review article. *Int. J. Remote Sensing*, 1987, **8**(12), 1807–1827.
69. Milton, E. J., Schaepman, M. E., Anderson, K., Kneubühler, M. and Fox, N., Progress in field spectroscopy. *Remote Sensing Environ.*, 2009, **113**, 92–109.
70. *Analytical Spectral Devices: Field Spec. TM*, Technical guide, Boulder, Co, USA, 1999, 3rd edn.
71. Denoth, A., An electronics device for long term snow wetness recording. *Ann. Glaciol.*, 1994, **19**, 104–106.
72. <http://www.toikkaoy.com>
73. Negi, H. S. and Kokhanovsky, A., Retrieval of snow albedo and grain size using reflectance measurements in Himalayan basin. *Cryosphere*, 2011, **5**, 203–217.
74. Negi, H. S., Singh, S. K., Kulkarni, A. V. and Semwal, B. S., Field based spectral reflectance measurements of seasonal snow cover in the Indian Himalaya. *Int. J. Remote Sensing*, 2010, **31**, 2393–2417.
75. Negi, H. S., Kulkarni, A. V. and Semwal, B. S., Study of contaminated and mixed objects snow reflectance in Indian Himalaya using spectroradiometer. *Int. J. Remote Sensing*, 2009, **30**(2), 315–325.
76. Haertel, V. F. and Shimabukuro, Y. E., Spectral linear mixing model in low spatial resolution image data. *IEEE Trans. Geosci. Remote Sensing*, 2005, **43**(11), 2555–2562.
77. Rees, W. G., *Remote Sensing of Snow and Ice*, CRC Press, Taylor & Francis Group, 2006.
78. Kokhanovsky, A. A. and Zege, E. P., Scattering optics of snow. *Appl. Opt.*, 2004, **43**, 1589–1602.
79. Singh, S. K., Kulkarni, A. V. and Chaudhary, B. S., Hyperspectral analysis of snow reflectance to understand the effects of contamination and grain size. *Ann. Glaciol.*, 2010, **51**(54), 83–88.
80. Singh, S. K., Kulkarni, A. V. and Chaudhary, B. S., Spectral characterization of soil and coal contamination on snow reflectance using hyper-spectral analysis. *J. Earth Syst. Sci.*, 2011, **120**(2), 321–328.
81. Painter, T., Comment on Singh and others, Hyper-spectral analysis of snow reflectance to understand the effects of contamination and grain size. *J. Glaciol.*, 2011, **57**, 183–185.
82. Negi, H. S. and Kokhanovsky, A., Retrieval of snow grain size and albedo of western Himalayan snow cover using satellite data. *Cryosphere*, 2011, **5**, 831–847.
83. Negi, H. S., Jassar, H. S., Saravana, G., Thakur, N. K. and Snehmani, G. A., Snow-cover characteristics using Hyperion data for the Himalayan region. *Int. J. Remote Sensing*, 2013, **34**(6), 2140–2161.
84. Kokhanovsky, A., Spectral reflectance of solar light from dirty snow: a simple theoretical model and its validation. *Cryosphere*, 2013, **7**, 1325–1331.

ACKNOWLEDGEMENTS. We thank SASE, DRDO for providing the field and cold laboratory facilities to carry out spectroradiometer experiments. We also thank A. Ganju, Director, SASE, Chandigarh for encouragement and support and Space Applications Centre, ISRO, Ahmedabad for collaborative joint field campaigns.